Turk J Phys
34 (2010) , 97 – 106.
© TÜBİTAK
doi:10.3906/fiz-1002-19

Photocurrent and surface recombination mechanisms in the $In_xGa_{1-x}N/GaN$ different-sized quantum dot solar cells

Hossein MOVLA[1], **Foozieh SOHRABI**[2], **Jafar FATHI**[2], **Hassan BABAEI**[3]
Arash NIKNIAZI[1], **Khadije KHALILI**[4], **Nima ES'HAGHI GORJI**[5]
[1]*Department of solid state physics, Faculty of Physics, University of Tabriz, Tabriz 51566, IRAN*
e-mail: h.movla@gmail.com
[2]*Department of atomic and molecular physics, Faculty of Physics, University of Tabriz, Tabriz 51566, IRAN*
[3]*Department of Theoretical physics, Faculty of Physics, University of Tabriz, Tabriz 51566, IRAN*
[4]*Photonics Group, Research Institute for Applied Physics and Astronomy (RIAPA), University of Tabriz, Tabriz 51665-163, IRAN*
[5]*Department of optics and laser, Technical and Engineering Faculty of Bonab, Bonab 55517, IRAN*

Received 19.02.2010

Abstract

We present a p-i-n structured solar cell with stacked layers of $In_xGa_{1-x}N$ Quantum Dots (QDs) with different indium composition. The photocurrent and surface recombination processes are investigated in the i-region. We have shown that the QDs in the i-region can play the role of both generation or recombination centers. The photocurrent has been calculated by self-consistent method to solve continuity equation of charge carriers in the layers of the i-region. By changing the Indium composition in $In_xGa_{1-x}N$ QDs, the band gap of QDs varies and therefore provides a considerable overlapping with solar spectrum. Proposed SC with different-sized QDs and different Indium composition leads to absorption of a desirable wavelength range of solar spectrum and therefore a "rainbow" solar cell can be designed.

Key Words: p-i-n Solar Cells, $In_xGa_{1-x}N$ Quantum dots, photocurrent, surface recombination rate.

1. Introduction

Solar photons which have the energy range from about 0.5 to 3.5 eV are known as solar spectra, and direct wide band gap group of III-nitrides such as InGaN (0.77–3.44 eV) are the bases of modern optoelectronic

devices, e.g. laser, light emitting diodes and sensors [1, 2], which can be used in solar cells. The band gap of $In_xGa_{1-x}N$ depends on x and varies from 0.77 to 3.44 eV for the range of $x = 0$ to 1. $In_xGa_{1-x}N$ has a good lattice match with GaN [3, 4]. $In_xGa_{1-x}N$ absorbance spectra and the solar spectra are illustrated in Figure 1; note the considerable overlap between the spectrums.

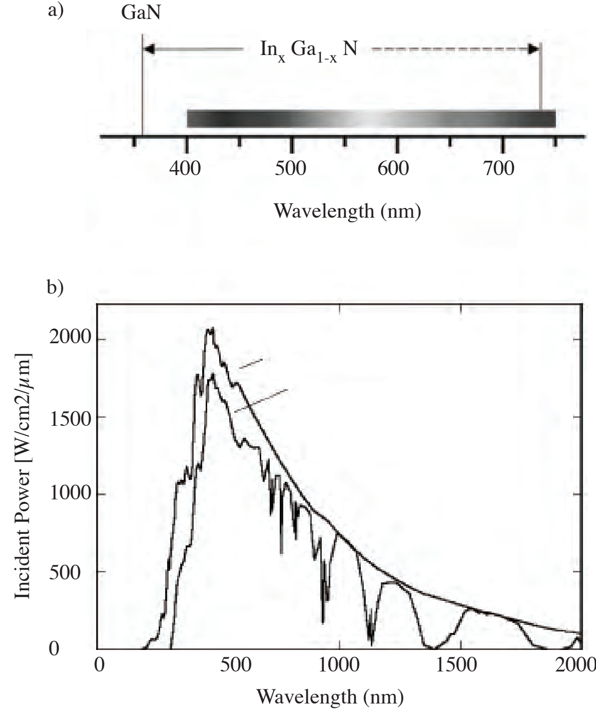

Figure 1. Continuum variations of $In_xGa_{1-x}N$ band gaps in terms of x and overlapping with (a) solar spectrum and (b) solar spectrum at AM 0 and AM 1.5.

Other advantages of Nitride quantum dots (QDs) which have attracted great interest are the low effective mass of electrons and holes, high carrier mobility, high peak and saturation velocities, high absorption coefficients, radiation tolerance and long carrier lifetime[5, 6, 7, 8].

QDs with appropriate band alignment have potential to increase the solar energy conversion efficiency over 63% by the intermediate band effect [9]. QDs can help with additional generation-recombination centers or form the intermediate band which originates from the overlap between the electrons' confined states in the dots [10, 11]. The intermediate bands arise from the energy levels of the electrons confined within the QDs. These energy levels can vary due to size variations of the QDs. This provides a desirable overlap between QD energy levels and solar spectrum and proposed for the performance enhancement of the solar cells which leads to the idea of quantum dot solar cells [9, 12].

The efficiency of solar cell strongly depends on types of QDs and barrier, QD size, QD constituent composition in ternary QDs, QDs volume density and QDs' band gap difference with the barrier.

There is a proposition of a multi-stacked structure of different-sized InGaN QDs in the i-region of GaN p-i-n solar cell for calculation of photocurrent density under AM=1.5 standard condition. This structure can be fabricated by MBE or MOCVD techniques which yield a high dot density, good dot uniformity and dot-sized

alignment.

We stacked 20 layers of QDs with sizes from 6 to 14 nm inserted in the i-region. By using the QDs in p-i-n solar cells, the obtainable photocurrent density and effective surface recombination rate are calculated by efficiently harvesting a large part of the useful spectrum of sunlight. It is possible to achieve a high density QD in active layer of p-i-n solar cells which provides an intermediate band for efficient photovoltaic effects.

2. Theory

In this paper, we developed further a model that has been used in our past studies [13]. Figure 2 illustrates the present proposed structure of solar cell. The sandwich structure of GaN barrier layers arranges $In_x Ga_{1-x}N$ QD layers in the i-region. The average surface density of QDs is assumed to be N_s. Each layer of the same sized QDs supports only one confined state of electron. Different-sized QDs in different layers of SC efficiently overlap with the large part of the useful spectrum of sunlight, and in this way rainbow SCs can be designed.

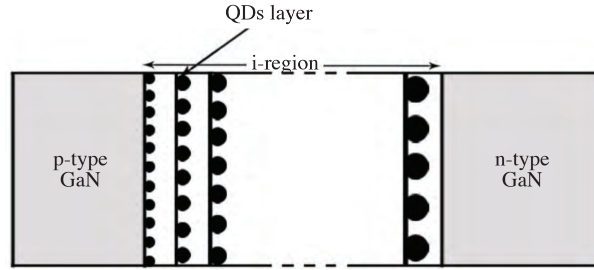

Figure 2. The p-i-n quantum dot Solar cell structure with different sized QDs in each layer.

In such systems, the processes of photon absorption, carrier relaxation and recombination can be distinguished by the Shockley-Read-Hall model (SRH). These processes are important to photovoltaic energy conversation. Rates for the Mth layer, as diagrammed in Figure 3, are as follows.
(1) Capture of an electron by QDs from adjacent barrier regions:

$$C_m = \alpha n(z,m) N_s (1 - f_n^m); \tag{1}$$

(2) Escape of electrons from QDs of interested layer:

$$E_m = \beta N_s f_n^m; \tag{2}$$

(3) Recombination in QDs:

$$R_m = \gamma N_s (f_n^m - f_{n0}); \tag{3}$$

(4) Optical generation in QDs:

$$G_m = \eta N_s (1 - f_n^m). \tag{4}$$

These rates (per unit area, per unit time) depend on the dot filling and on QD layer position within the i-region. Here, α , β, γ and η are the capture, escape, recombination and generation coefficients, respectively. f_n^m is the average of non-equilibrium population of QDs in the Mth layer, f_{n0} is the equilibrium of Fermi-Dirac occupation probability, $n(z,m)$ is density of free electrons at the frontal surface of Mth layer with position of $z_m = (m-1)d$.

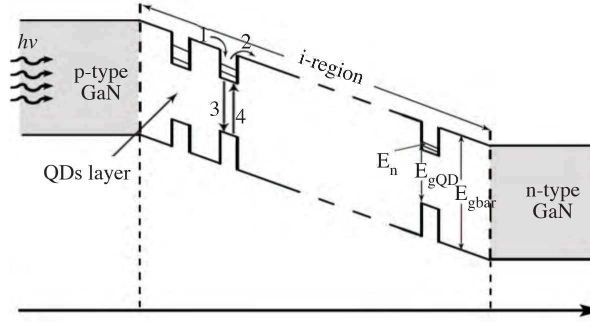

Figure 3. Energy-band diagram of p-i-n QD solar cell and generation-recombination processes in QDs for one type of carriers. Depletion layers in p and n layers are neglected.

Under steady state operation, the following condition should be applied:

$$(C_m - E_m) + (R_m - G_m) = 0. \tag{5}$$

Under dark condition, where $R_m = G_m = 0$, the above equation can be changed to

$$\alpha n_0(1 - f_{n0}) - \beta f_{n0} = 0, \tag{6}$$

where the equilibrium density of electrons and population probability of QDs are given by the equations

$$n_0 = N_c \exp\left(\frac{E_f - E_c}{kT}\right), \quad f_{n0} = \left[1 + \exp\left(\frac{E_n - E_f}{kT}\right)\right]^{-1}, \tag{7}$$

where E_c, E_f, kT and E_n are conduction band edge, Fermi energy, thermal energy and the confinement energy in the QD, respectively. Therefore the coefficient α can be written

$$\beta = n_1 \alpha, \tag{8}$$

where

$$n_1 = N_c \exp\left(-\frac{E_c - E_n}{kT}\right). \tag{9}$$

Solving equation (5) using equation (8), the population factor f_n^m can be obtained as

$$f_n^m = \frac{-\alpha n(z,m) + \gamma f_{n0} + \eta}{-\alpha[n(z,m) + n_1] + \gamma + \eta}. \tag{10}$$

The effective surface recombination rate on the plane of the Mth QD's layer is defined by

$$U_s^m = C_m - E_m. \tag{11}$$

Finally we use equation (10) to obtain U_s^m:

$$U_s^m = \alpha N_s \frac{[n(z,m)(n_1 + \gamma - \gamma f_{n0} + \alpha n_1) - n_1 \gamma f_{n0} - \eta]}{-\alpha[n(z,m) + n_1] + \gamma + \eta}. \tag{12}$$

The effective surface recombination rate from this expression may have either positive or negative values. For the positive values of U_s^m, QDs behave as recombination centers; while for the negative values they behave as generation centers. Such behavior strongly depends on the free electron concentration near the given layer specially if we express the capture, recombination and generation rates, respectively by

$$\alpha_c = \frac{1}{N_D \tau_c}, \gamma = \frac{1}{\tau_r}, \eta = \frac{1}{\tau_g}. \tag{13}$$

Here, N_D is the volume concentration of QDs. U_s^m depends on free electron density and varies from one layer to another. The capture rate also can be described by the simple relation $\alpha_c = \sigma v$. Here, σ is the electron capture cross-section of the QD, and v is the average thermal velocity of electrons at room temperature and is about 107 cm/s [14].

The total generated photocurrent in the i-region, by taking into account the existence of QDs through the effective surface recombination rates (U_s^m), can be calculated self consistently solving the current continuity equation for inter-layer regions.

The electron current density in a semiconductor consists of two components, namely the drift and diffusion currents, are given by the relations

$$j_n = q\mu_n E + qD_n \nabla n, \tag{14}$$

$$-\mu_n E \frac{dn(z,m)}{dz} = F(\lambda)\alpha(\lambda)\exp[-\alpha(\lambda)z], \tag{15}$$

where, q, $\alpha(\lambda)$, μ_n and E are the electron charge, light absorption coefficient, electron mobility of barrier region and electric field, respectively.

Now, let us calculate the current in the first interval $0 \le z \le d$. We neglect the drift component and recombination rate in barriers. Free electron density $n(z,1)$ in the first inter-dot region (between the first and second QD layers), for the incident light of wavelength λ and flux $F(\lambda)$ [14], is obtained via the equation

$$-\mu_n E \frac{dn(z,1)}{dz} = F(\lambda)\alpha(\lambda)\exp[-\alpha(\lambda)z]. \tag{16}$$

Solving equation (16) with respect to the $n(z,1)$, we get the relation

$$n(z,1) = C_1 + \frac{1}{\mu_n E} F(\lambda)\exp[-\alpha(\lambda)z]. \tag{17}$$

By defining $L_n = 2D_n/\mu_n E$ as electron diffusion length and replacing it in equation (17), we get

$$n(z,1) = C_1 + \frac{L_n}{2D_n} F(\lambda)\exp[-\alpha(\lambda)z], \tag{18}$$

where D_n is the diffusion coefficient. Constant C_1 is calculated by considering the boundary condition arising from adjoining the p-emitter to the i-region:

$$q\frac{2D_n}{L_n}n(z=0,1) = j_n^0 - qU_s^1. \tag{19}$$

Here, $j_n^0 = 22\ \text{mA/cm}^2$ is the electron current density at the edge of p-emitter region [14]. By obtaining C_1, we can find the photocurrent generated in the first inter-dot region, especially at the layers' interface ($z = d$). Considering carrier continuity, it is obvious that incoming current will be equal to the outgoing current from the first inter-dot barrier region. Consequently, for other layers we have the relation

$$q\frac{2D_n}{L_n}n(z,m) = j_n^{m-1} - qU_s^m. \tag{20}$$

This method is applied to other inter-dot regions to calculate the j_n^m in all layers of the i-region. The total collected photocurrent at the end of Mth layer (as the last layer) from the intrinsic region, including photocurrents generated in both inter-dot regions and QD layers is formulated by the equation

$$j_n^m = j_{n\,\text{QD}}^m + qF(\lambda)(1 - \exp(-\alpha(\lambda)d). \tag{21}$$

The first term is generated from QD layers and the second term is created by inter-dot regions.

3. Results and discussion

This part shows the simulation results of the proposed structure for the solar cell. Used physical constants are listed in Table 1 and the capture, recombination and generation times are estimated as physical parameters in the model [14, 15, 16, 17, 18, 19, 20, 21].

Table 1. The parameters of the GaN/InGaN

Parameter	Unit(s)	InGaN	GaN	Reference
L_n	cm	–	2×10^{-5}	[14]
μ_n	$\text{cm}^2/\text{V·s}$	–	760	[15]
D_n	–	–	0.38	–
S_n	cm/s	–	3×10^4	[16]
$E_{g(\text{Barr})}$	eV	–	3.44	[17]
$E_{g(\text{QD})}$	eV	$1.7 - 2.49$	–	[3]
$\alpha(\lambda)$	cm^{-1}	–	$(15 - 60) \times 10^2$	[18]
σ_{QD}	cm^2	$10^{-10} - 10^{-12}$	–	[19, 20]
N_{D}	cm^3	$10^{17} - 10^{20}$	–	–
σ_{abs}	cm^2	$10^{-14} - 10^{-16}$	–	–
$\alpha_{\text{abs}}(\omega)$	cm^{-1}	10^{-6}	–	[21]
N_s	cm^{-2}	10^{11}	–	–

By using given ranges of σ and N_{D}, capture time is obtained in the range of $\tau_{\text{c}} \sim 50 - 330$ ps. By using physical parameters in Table 1, typical recombination lifetime can be estimated in the range of $\tau_{\text{r}} \sim 1 - 150$ ps.

Recombination lifetime depends on the amplitude of electrical field in the i-region ($E \sim 0.05 - 0.2$ MV/cm) [21, 22].

For the optical generation rate, $\eta = 800 - 1750$ s^{-1} is chosen, which can be determined by the following equation [12]:

$$\eta = \frac{1}{\tau_c} \int_{E_{g(\mathrm{QD})}}^{E_{g(\mathrm{Barr})}} \sigma_{\mathrm{abs}} \Phi(\hbar\omega) d\omega, \tag{22}$$

where σ_{abs} is the optical absorption cross section of quantum dots and can be related to absorption coefficient $\alpha_{\mathrm{abs}}(\omega)$ of QDs by $\sigma_{\mathrm{abs}}(\omega) = \alpha_{\mathrm{abs}}(\omega)/N_D$ [23, 24]. $\Phi(\hbar\omega)$ is incident solar photon flux, under condition of standard 1.5 AM.

The results of the Photocurrent density and effective surface recombination rate as a function of the number of QD layers in the i-region (M) and for three different lifetimes are shown in Figures 4, 5, 6, 7, 8 and 9.

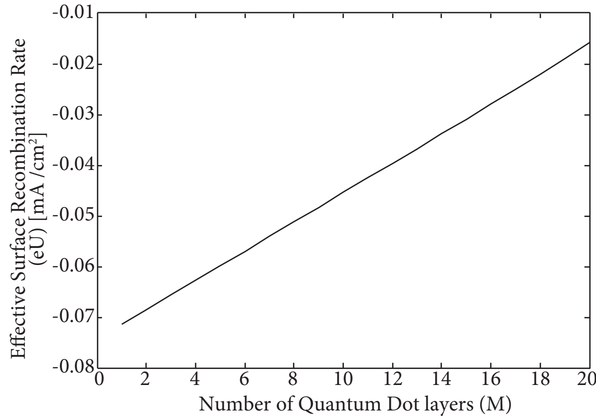

Figure 4. Effective surface recombination rate versus the number of quantum dot layers (M) when $\tau_r = 50$ ps.

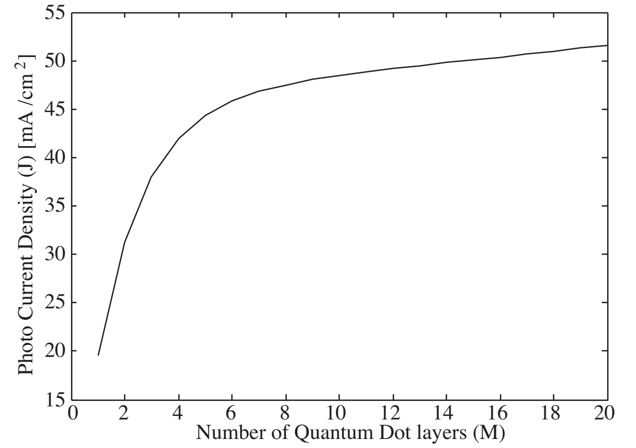

Figure 5. Photocurrent density versus number of quantum dots layers when $\tau_r = 50$ ps.

Figure 4 shows the effective surface recombination rate U and Figure 5 shows photocurrent density (J) with $\tau_r = 50$ ps. The photocurrents increase with respect to the number of QD layers and also the generation center behavior of all QD layers are illustrated. Because of the negative value of effective surface recombination rate, QDs play the role of generation centers.

Figure 6 shows that effective surface recombination rate U and Figure 7 shows the increase of current density J as a function of number of QD layers, where $M_{\mathrm{QD}} \leq 10$ layers behave as generation and $11 \leq M_{\mathrm{QD}} \leq 20$ QDs behave as recombination centers. It is clear that the current density slope decreases because of the positive value of surface recombination rate for $11 \leq M_{\mathrm{QD}} \leq 20$ layers.

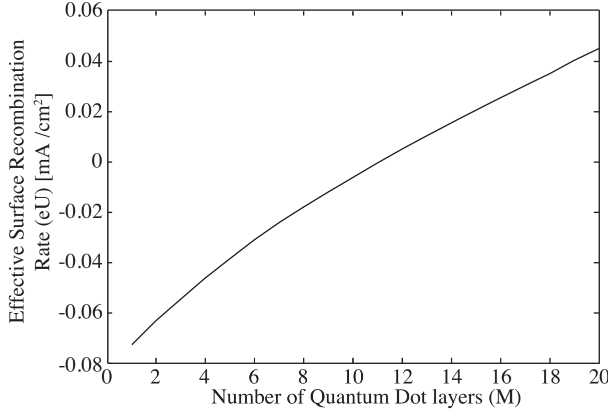

Figure 6. Effective surface recombination rate versus number of quantum dot layers (M) when $\tau_{\rm r} = 1$ ns.

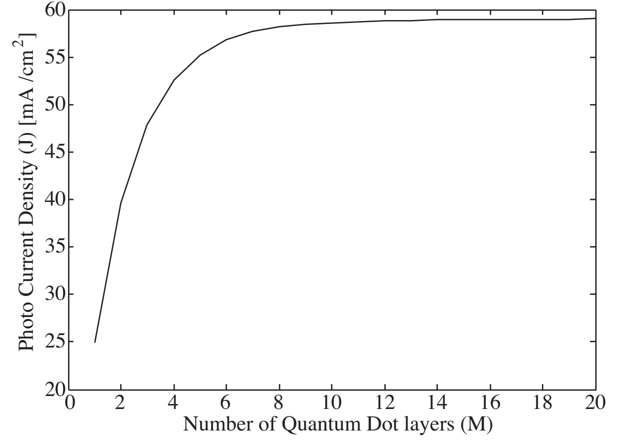

Figure 7. Photocurrent density versus number of quantum dot layers for $\tau_{\rm r} = 1$ ns.

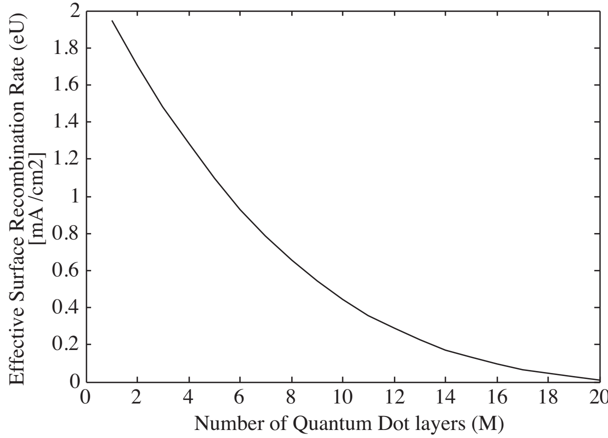

Figure 8. Effective surface recombination rate versus number of quantum dot layers (M) for $\tau_{\rm r} = 2$ ps.

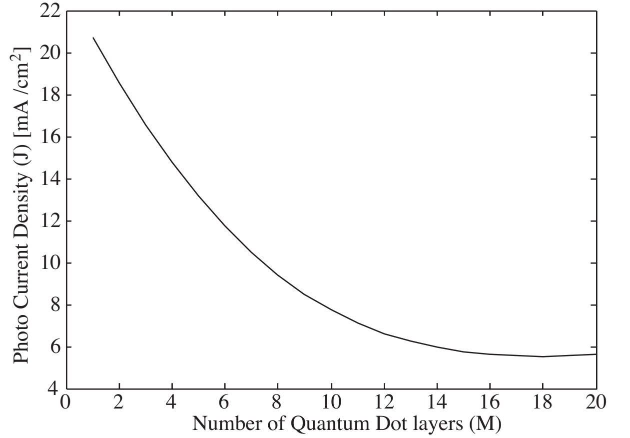

Figure 9. Photocurrent density versus number of quantum dot layers for $\tau_{\rm r} = 2$ ps.

Figure 8 illustrates effective surface recombination rate U and Figure 9 shows the current density J versus the number of QD layers for a very low recombination time in QDs, $\tau_{\rm r} = 2$ ps. For this low value of recombination time, the number of captured carriers would be higher than escaped ones from QDs, so QDs take part as recombination centers and the surface recombination rate will get a positive value. Because the QDs play the role as recombination centers, the density of carriers decreases from layer to layer and so the surface recombination rate decreases versus QDs layers. Also, it's seen from Figure 9 that current density follows the surface recombination rate changes.

Photocurrent densities for three different lifetimes and photocurrent for $N_s = 0$ are shown in Figure 10. Comparison of Photocurrent densities shows that the current density will increase by enlarging the intrinsic region of p-i-n SCs without any QDs. Also, it is shown that stacked layers of QDs can increase the current density of solar cell by absorbing lower energy photons. However, we should consider the carrier lifetime value of QDs to increase the current density.

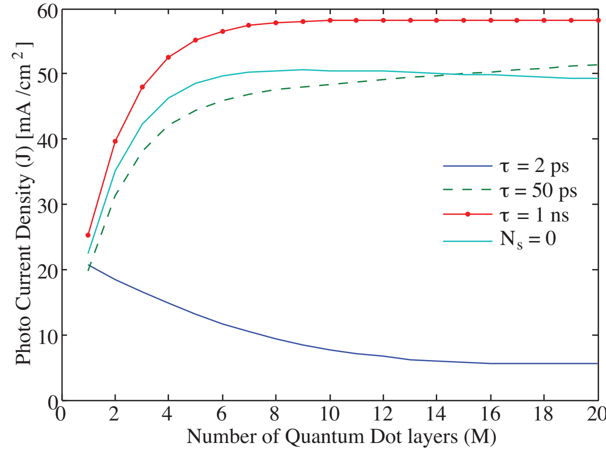

Figure 10. Photocurrent density versus M, for $\tau_{\mathrm{r}} = 2$ ps, 50 ps and 1 ns, compared with the photocurrent without quantum dots ($N_{\mathrm{s}} = 0$).

It is shown that using QDs in the active region, from small-sized QDs adjacent the anode, and large-sized QDs near the cathode, by considering the capture and escape speed processes as an important parameter, QD concentration, QD arrangement, layer thickness and the type of barrier leads to increase in the photocurrent density and the power conversion efficiency of p-i-n SCs, photon absorption in the long-wavelength part of the spectrum and increase in the power conversion efficiency.

4. Conclusion

We have designed a rainbow solar cell by arranging multi-stacked layers of different-sized $\mathrm{In}_x\mathrm{Ga}_{1-x}\mathrm{N}$ QDs ($L = 6$ nm to 14 nm) with different In composition in the i-region of a p-i-n structure. The photocurrent density and effective surface recombination rate are calculated for $M = 20$ layers, where small QDs are located closer to p electrode and the large QDs are closer to n electrode. By using Different-sized QDs with different In composition, a wide range of solar spectra can be harvested in the range of 0.5–3.5 eV. This is a possible route to increase the performance of solar cells and get the maximum attainable efficient performance. However, we can enhance its performance by considering the real conditions in future work.

Acknowledgements

The authors would like to express his thanks to Mr. Mohammad Soltanpour for grateful helps to prepare this paper.

References

[1] J. Wu, W. Walukiewicz, K. M. Yu, J. W. Ager III, E. E. Haller, H. Lu, William J. Schaff, Y. Saito and Y. Nanishi, *Appl. Phys. Lett.*, **80**, (2002), 3967.

[2] J. Piprek, *Nitride Semiconductor Devices, Principles and Simulation,* (Wiley, Berlin, 2006).

[3] T. Takeuchi, H. Amano and I. Akasaki, *Jpn. J. Appl. Phys.*, **80**, Part 1, 39, (2000), 413.

[4] Z. Dridi, B. Bouhafs and P. Ruterana, *Semicond. Sci. Technol*, **18**, (2003), 850.

[5] Y. Nanishi, Y. Saito and T. Yamaguchi, *J. Appl. Phys.*, **42**, (2003), 2549.

[6] U. K. Mishra, P. Parikh and Y. F . Wu, *Proceedings of the IEEE*, **90**, (2002), 1022.

[7] O. Ambacher, B. Foutz, J. Smart, J. R. Shearly, N. G. Weimann, K. Chu, M. Murphy, A. J. Sierakowski, W. J. Schaff, L. F. Eastman, R. Dimitrov, A. Mitchell and M. Stutzmann, *J. Appl. Phys.*, **87**, (2000), 3222.

[8] J. Wu, *J. Appl. Phys.*, **94**, 7, (2003), 4457.

[9] A. Luque and A. Marti, *Phys. Rev. Lett.*, **78**, (1997), 5014.

[10] L. Caudra, A. Marti and A. Luque, *Thin Solid Films*, **593**, (2004), 451.

[11] A. J. Nozik, *Physica E.*, **14**, (2002), 115.

[12] V. Aroutiounian, S. Petrosyan, A. Khachatryan and K. Touryan, *J. Appl. Phys.*, **89**, (2001), 2268.

[13] N. E. Gorji, H. Movla, F. Sohrabi, A. Hosseinpour, M. Rezaei and H. Babaei, *Phys. E*, **42**, (2010), 2353.

[14] Z. Z. Bandi, P. M. Bridger, E. C. Piquette and T. C. McGill, *Appl. Phys. Lett*, **73**, (1998), 3276.

[15] J. G. Kim, A. C. Frenkel, H. Liu and R. M. Park, *Appl. Phys. Lett.*, **65**, (1994), 91.

[16] R. Aleksiejunas, M. Sudzius, V. Gudelis, T. Malinauskas, K. Jarasiunas, Q. Fareed, R. Gaska, M. S. Shur, J. Zhang, J. Yang, E. Kuokstis, and M. A. Khan, *Phys. stat. sol. (c)*, **0**, (2003), 2686.

[17] B. Monemar, *Phys. Rev. B*, **10**, (1974), 676.

[18] O. Ambacher, W. Rieger, P. Ansmann, H. Angerer, T. D. Moustakas and M. Stutzman, *Sol. State Commun.*, **97**, (1996), 365.

[19] S. K. Zhang, H. J. Zhu, F. Lu, Z. M. Jiang and X. Wang, *Phys. Rev. Lett.*, **82**, (1999), 3340.

[20] O. Engstrom, M. Kaniewska, Y. Fu, J. Piscator and M. Malmkvist, *Appl. Phys. Lett.*, **85**, (2004), 2908.

[21] T. Ouisse and A. G. Nassiopoulou, *Euro. Phys. Lett.*, **51**, (2000), 168.

[22] S. Corni, M. Braskeon, M. Lindberg, J. Olsen and D. Sundholm, *Phys. Rev. B*, **67**, (2003), 045313.

[23] V. Aroutiounian, S. Petrosyan and A. Khachatryan, *Sol. Energy Mater. Sol. Cells.*, **89**, (2005), 165.

[24] D. berg, M. Grundmann and N. Ledentsov, *Quantum Dot Heterostructures*, (Wiley, New York, 1999).